Journal of Power Sources 316 (2016) 207–214

Contents lists available at ScienceDirect

Journal of Power Sources

journal homepage: www.elsevier.com/locate/jpowsour

Integrated plasmonic and upconversion starlike Y_2O_3:Er/Au@TiO_2 composite for enhanced photon harvesting in dye-sensitized solar cells

Fanli Meng [a], Yi Luo [a], Yali Zhou [a], Jinwen Zhang [a], Yanzhen Zheng [a, b, **], Guozhong Cao [c], Xia Tao [a, *]

[a] State Key Laboratory of Organic-Inorganic Composites, Beijing University of Chemical Technology, Beijing 100029, China
[b] Research Center of the Ministry of Education for High Gravity Engineering & Technology, Beijing University of Chemical Technology, Beijing 100029, China
[c] Department of Materials Science and Engineering, University of Washington, Seattle, WA 98195, USA

HIGHLIGHTS

- A 3D starlike upconversion composite with plasmon-enhanced emission is prepared.
- This composite is introduced into the scattering layer of DSSC.
- Both charge transport and light harvesting are improved.
- Photoelectric conversion efficiency is improved from 6.77% to 8.62%.

GRAPHICAL ABSTRACT

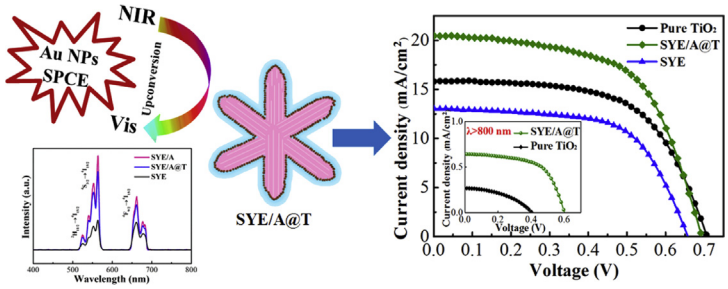

ARTICLE INFO

Article history:
Received 23 September 2015
Received in revised form
19 January 2016
Accepted 8 March 2016
Available online 4 April 2016

Keywords:
Dye-sensitized solar cell
Upconversion
Plasmon-enhanced emission
Photovoltaic performance

ABSTRACT

A plasmon-enhanced upconversion composite Y_2O_3:Er/Au@TiO_2 (SYE/A@T) with a three-dimensional starlike morphology is prepared and then mixed with submicron TiO_2 (200 nm) to form a multifunctional scattering layer in TiO_2-based dye-sensitized solar cells (DSSCs). In such starlike micronsized upconverter, Au nanoparticle-assisted plasmon effect can intensify the upconversion emission of Y_2O_3:Er, and simultaneously TiO_2 coating can improve the charge transport within SYE/A@T. Therefore, the SYE/A@T shows extended light-absorbing range to near-infrared region and improved light-scattering ability, leading to an improved photovoltaic performance of DSSCs. With the optimum mixing ratio, a conversion efficiency of 8.62% is attained, which is a significant improvement of 27.6% compared with the cell without adding SYE/A@T. Our work provides a feasible strategy to prepare an upconversion composite with plasmon-enhanced emission and enable this composite to accommodate the DSSCs system and improve the conversion efficiency of DSSCs.

1. Introduction

Dye-sensitized solar cells (DSSCs) have drawn considerable attention since their advent in 1991 [1] due to their characteristics of low cost, ease of production, and high conversion efficiency

* Corresponding author.
** Corresponding author. State Key Laboratory of Organic-Inorganic Composites, Beijing University of Chemical Technology, Beijing 100029, China.
E-mail address: taoxia@yahoo.com (X. Tao).

http://dx.doi.org/10.1016/j.jpowsour.2016.03.032
0378-7753/

[2–6]. Typically, a sandwich-structured DSSC device is composed of a dye-sensitized TiO_2 film photoanode, a platinum counter electrode, and an I^-/I_3^- redox couple electrolyte [7]. In a DSSC, incident photons are absorbed by dye molecules, and then dye molecules inject electrons into the conduction band of TiO_2 upon optical excitation [7]. However, the widely used commercial dye sensitizers, such as N719 and N3, exhibit limited absorption wavelength ranges below 700 nm, owing to their inherent optical bandgaps of over 1.8 eV. Thus, approximately 50% of the total solar energy flux in infrared light (NIR) could not be harnessed by conventional ruthenium dyes, and hence limit the optoelectronic conversion efficiency of device, leaving plenty of room to improve the performance of DSSCs through dye molecular sensitizers exploitation, as well as composition modification of photoelectrode [8]. One commonly used way to broaden the spectral response of DSSCs to NIR region or even infrared region is to developing panchromatic dye sensitizers [9,10] or cosensitizing by multiple dyes with complementary absorption spectra [5,11–15]. However, most new designed panchromatic dye could not absorb visible light as strongly as conventional ruthenium dyes, and multiple dyes mostly involve complicated cosensitization procedures.

Another feasible strategy to overcome this limitation is to use upconversion (UC) luminescent materials, which can convert light from NIR (>900 nm) to visible (<750 nm) region [16,17]. UC materials have attracted wide notice from researchers because of their great potential for optical devices, bio-analysis, medical therapy, display technologies, and light harvesting [18]. For photovoltaic cells, utilizing UC materials can break the Shockley–Queisser limit of all single-junction cells [18], and then improve the efficiencies of various photovoltaic cells [19,20]. It has been reported that incorporation of UC materials (such as LaF_3: Yb/Er, YF_3:Yb/Er, YOF:Yb/Er, $NaYF_4$:Yb/Er, and Y_2O_3:Er, etc.) into TiO_2 or ZnO nanocrystallite films could extend the absorption region of DSSCs [21–25]. However, UC materials would suffer from the fundamental drawbacks of relative weak emission intensity of UC materials related to low quantum yield of every UC process [26]. Recently, it was reported that localized surface plasmon resonance (LSPR) effect from nanosized noble metal (such as Au and Ag NPs) is capable of enhancing the emission of UC materials [27–32]. To date, plasmon-enhanced UC materials have been introduced in DSSCs devices to enhance light absorption and photocurrent generation [33]. However, it is worth pointing out that incorporation of these materials within TiO_2 film would inevitably introduce surface defects and ligands with high-energy vibrational modes and then act as effective trapping centers and trap large part of photo-induced electrons, hence leading to severe electron-hole recombination and a heavy loss of photocurrent [34–36]. Such a drawback has become a major obstacle for applying UC materials in DSSCs internally [37,38]. To overcome this limitation, Shan [38] and Ramasamy [39] proposed to coat an external light-reflecting layer consisting of UC NPs on the back of platinum electrode in DSSCs to avoid the recombination effect, and achieved an increase of efficiency ~10.2%. For internal scattering layer, coating a shell with TiO_2 or SiO_2 is a conventional way to eliminate surface defects. Liang designed a highly uniform core/double-shell structured β-$NaYF_4$:Yb,Er@SiO_2@TiO_2 to effectively inhibit negative recombination effect [40].

This paper reports the design and synthesis of a plasmon-enhanced UC composite comprising a core of starlike Y_2O_3:Er (SYE) attached with Au NPs and a shell of anatase TiO_2 NPs. To balance the light scattering, electron transport and mechanical strength, the Y_2O_3:Er/Au@TiO_2 composite was mixed with TiO_2 submicron spheres (200 nm in diameter) to form a multifunctional hybrid scattering layer in TiO_2-based DSSC devices. The schematic of preparation process and configuration of photoanode film is shown in Fig. 1. The micron-sized three-dimensional (3D) SYE acts as an effective NIR upconversion and light scattering center, resulting in strong and broader absorption [25]. By attaching Au NPs, the NIR light can be more effectively converted to visible light *via* plasmon-enhanced UC and ultimately absorbed by the dye sensitizer. By coating TiO_2, the surface charge recombination on SYE is largely reduced and the dye-loading is increased.

2. Experimental

2.1. Materials

Yttrium nitrate hexahydrate ($Y(NO_3)_3 \cdot 6H_2O$), erbium nitrate pentahydrate ($Er(NO_3)_3 \cdot 5H_2O$) and 4-*tert*-butylpyridine (TBP) were obtained from Aladdin. TiO_2 (20 nm) paste for the transparent layer and TiO_2 (200 nm) paste for scattering layer were purchased from Wuhan Ge'ao Co. Ltd. Iodide (I_2), lithium iodide (LiI), 1, 2-dimethyl-3-propylimidazolium iodide (DMPII), chloroplatinic acid (H_2PtCl_6), chloroauric acid ($HAuCl_4$) and titanium tetrafluoride (TiF_4) were purchased from Sigma-Aldrich Co. Ltd. Dye sensitizer, *cis*-bis(isothicyanato)bis(2,2'-bipyridyl-4,4″-dis-carboxylato)-ruthenium(II)-bis-tetrabutylammonium (N719) were obtained from Solaronix. All other chemicals were purchased from Beijing Chemical Works and were used without further purification. All solutions used in this work were prepared with 18.2 MΩ cm^{-1} water produced by a reagent water system (Easy pure II, Barnstead).

2.2. Preparation of 3D starlike Y_2O_3:Er/Au composite

The 3D starlike Y_2O_3:Er (denoted as SYE) was prepared with a modified method reported by Lu et al. [25]. For preparation of 3D starlike Y_2O_3:Er/Au composite (denoted as SYE/A), 100 mg of as-prepared SYE powder was dispersed in 50 mL deionized H_2O and sonicated for 30 min at room temperature. Then, 0.1 mL of 1% $HAuCl_4$ solution was added to the mixture, followed by dropwise adding 2 mL of 0.1% $NaBH_4$ solution to react for 10 min with vigorous stirring. The resultant solution was centrifuged, and the precipitate was washed with deionized water several times and then dried at 80 °C in air overnight.

2.3. Preparation of 3D starlike Y_2O_3:Er/Au@TiO_2 composites

To construct core-shell structured 3D starlike Y_2O_3:Er/Au@TiO_2 composites (denoted as SYE/A@T), 100 mg of as-prepared SYE/A powder was dispersed in 60 mL solvent with an equal volume of H_2O: ethanol and then sonicated for 30 min at room temperature. Then, 2 mL of 40 mM TiF_4 solution was added to the above mixture, followed by being stirred for 30 min. Finally, the mixture was transferred to Teflon-lined autoclaves and heated to 180 °C for 6 h. The resultant solution was centrifuged, and the precipitate was washed with deionized water and anhydrous ethanol several times and then dried at 100 °C in air overnight. Finally, the obtained powder was calcined at 500 °C for 3 h. For comparison, composites without Er doped (denoted as SY/A@T) and without Au NPs attached (denoted as SYE@T) were also prepared with the same procedure.

2.4. DSSC device assembly

In order to obtain the paste for multifunctional scattering layer (denoted as MSL), the as-prepared SYE/A@T corresponding to mass-fraction levels varying from 10% to 25% with respect to the commercial TiO_2 (200 nm) were mixed added into the paste. To construct a photoelectrode, a TiO_2-SYE/A@T based MSL was covered on a TiO_2 (20 nm) transparent layer (denoted as TL) with a screen-printing method and then dried at 70 °C for 1 h, followed by

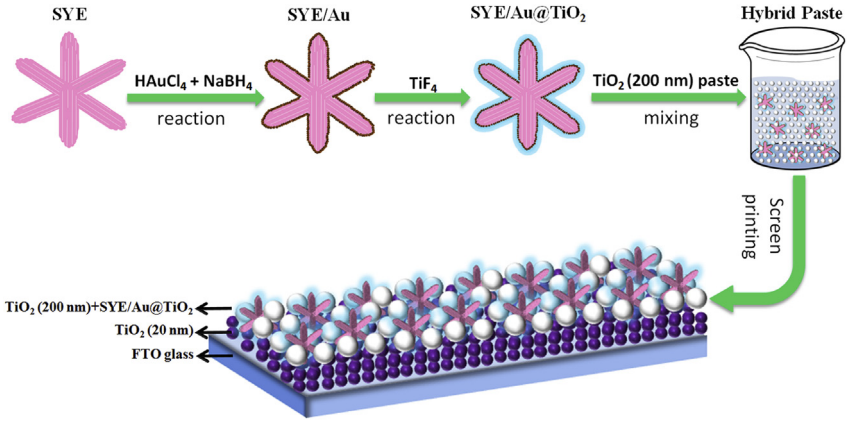

Fig. 1. Schematic diagram of experimental process for SYE/A@T and the photoanode configuration of DSSCs.

a programmed heating of 500 °C for 30 min. For comparison, SYE-, SYE@T-, and SY/A@T-mixed photoelectrodes together with pure TiO_2 photoelectrode (without adding upconversion species) were also prepared in parallel. The thicknesses of the photoelectrode films were all about 15 μm (11 μm for the TL and 4 μm for the MSL).

The resultant photoelectrodes were immersed into a 0.5 mM

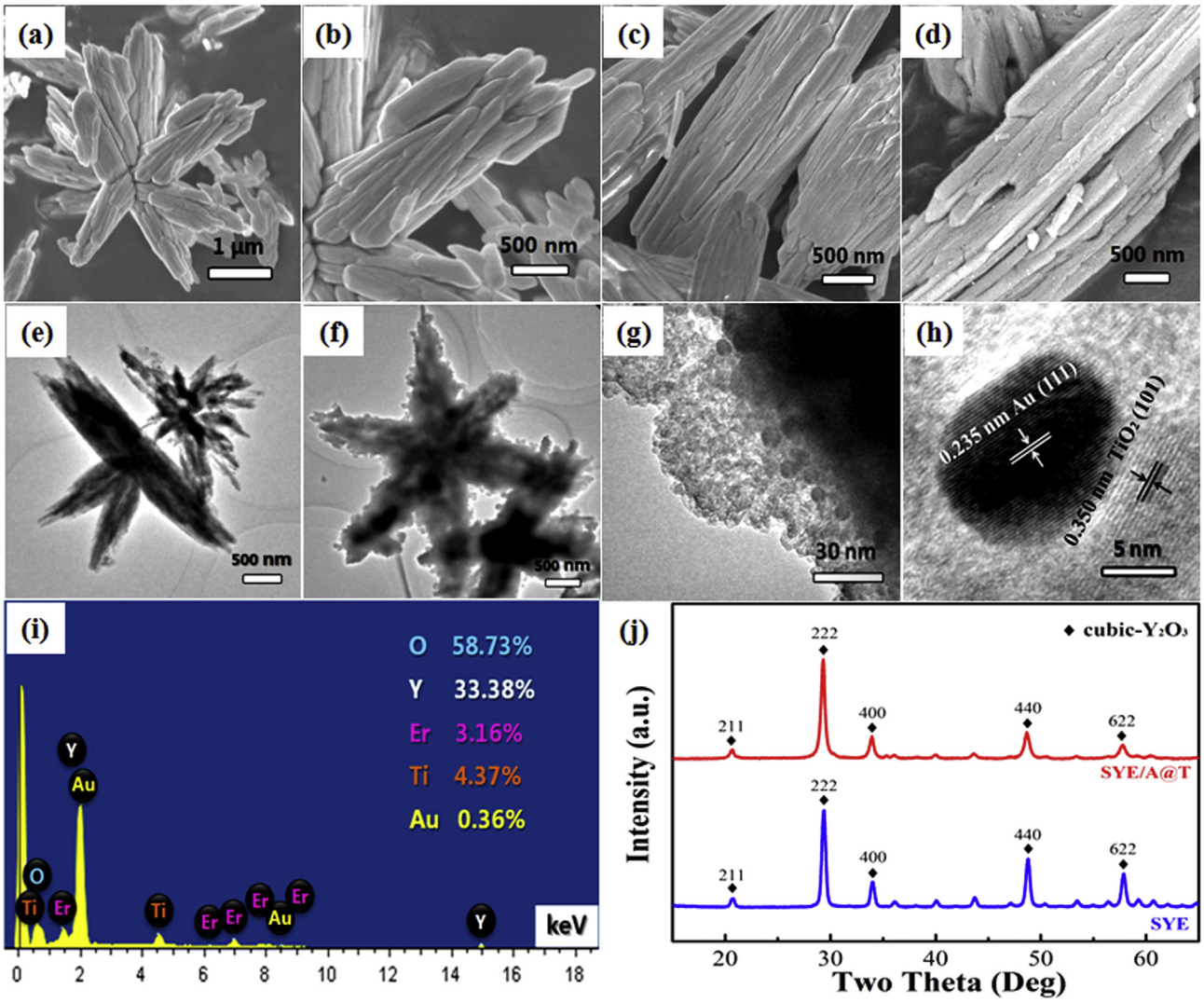

Fig. 2. SEM images of (a, b) SYE, (c) SY and (d) SYE/A@T. TEM images of (e) SYE and (f) SYE/A@T. (g, h) HRTEM images of SYE/A@T. (i) EDS spectrum of SYE/A@T with measured atom content. (j) XRD patterns of the prepared SYE and SYE/A@T.

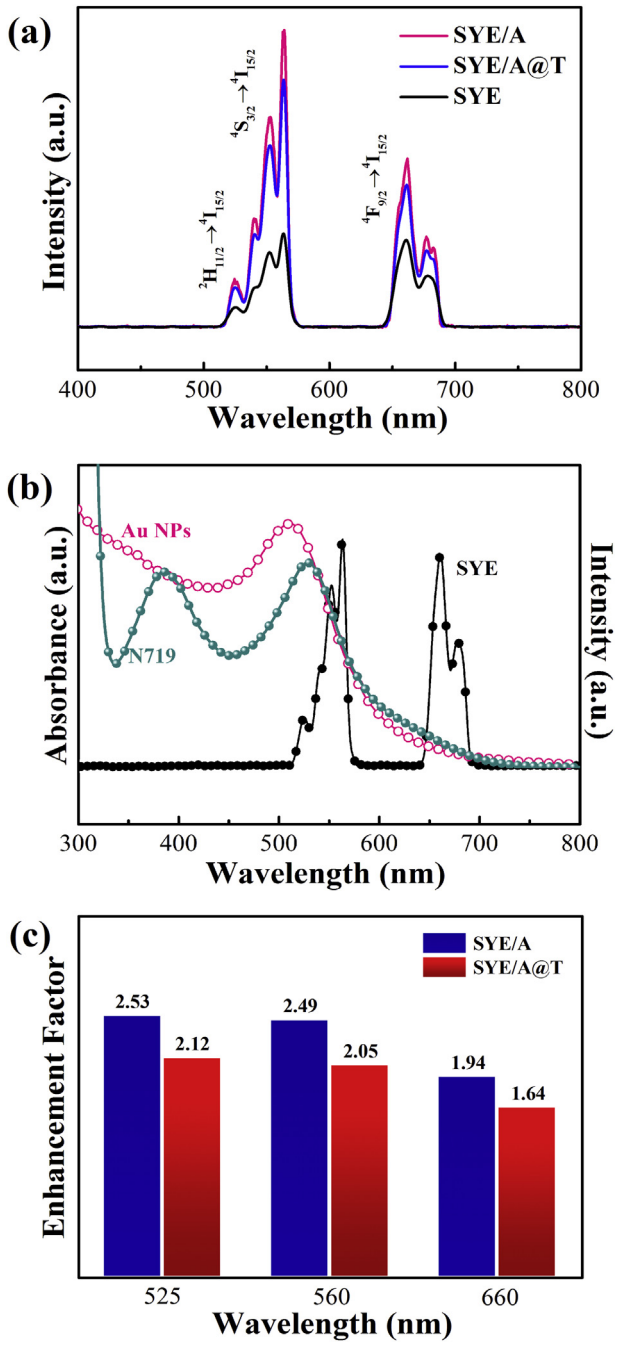

Fig. 3. (a) Photoluminescence spectra of SYE, SYE/A, and SYE/A@T. (b) Photoluminescence spectrum of SYE and UV–vis absorption spectra of Au NPs and N719. (c) Enhancement factors of UC intensities with respect to SYE for SYE/A and SYE/A@T.

N719 dye solution in anhydrous ethanol for 24 h at room temperature. The counter electrodes were prepared by drop-coating a 0.35 mM H_2PtCl_6 isopropanol solution on the FTO/glass substrate, followed by annealing at 400 °C for 15 min. Afterwards, the photoanode and the counter electrode were assembled into a sandwich cell using a surlyn sheet by automatic hot-pressing. Finally, the electrolyte consisting of 0.05 M I_2, 0.1 M LiI, 0.5 M DMPII, and 0.5 M TBP in acetonitrile was injected into the space between the counter electrode and the photoanode. The active area of a DSSC device exposed in light was 0.16 cm^2.

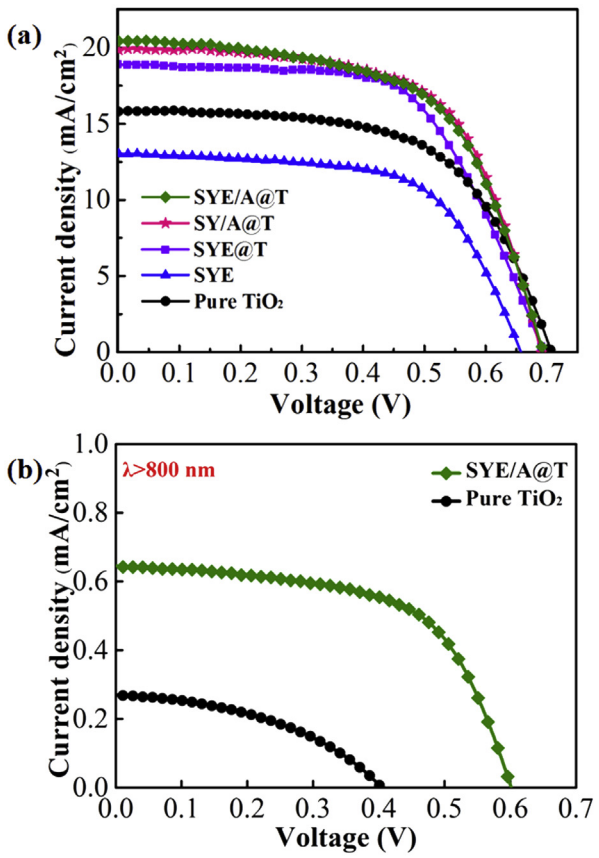

Fig. 4. *J–V* curves of DSSCs with different photoelectrodes under (a) AM1.5G light and (b) under an IR irradiation (λ > 800 nm) of 34.3 mW cm^{-2}.

2.5. Characterization

To detect the overall structure and morphology of as-synthesized composites and photoelectrodes, the samples were characterized by scanning electron microscopy (SEM) using a JEOL-6701F microscope equipped with an X-ray energy dispersive spectrometer (EDS). Transmission electron microscopy (TEM) and high resolution transmission electron microscopy (HRTEM) images were recorded on a JEOL 3010 microscope operated at 300 kV. The crystal structures were identified by X-ray power diffraction (XRD) using an X-ray diffractometer (X'Pert PRO MPD, Panalytical) with a Cu-Ka radiation. The absorption and diffuse reflectance spectra were measured by a UV–vis spectrophotometer (Lambda 950, Perkin Elmer). The upconversion photoluminescence spectra were performed on a spectrophotometer (FLS980, Edinburgh) with a CW NIR laser at 980 nm as the excitation source. Dye loading measurements were conducted by immersing the dye-sensitized photoanode films in 0.1 M NaOH solution and measuring the concentration of the desorbed dye by UV–vis absorption spectroscopy. Photovoltaic performances of DSSCs were characterized by measuring the current density-voltage (*J-V*) curves under air mass 1.5 global (AM 1.5G) light using a solar light simulator (Newport 69911, Stratford, CT, USA), and the data were recorded by an electrochemical workstation (CHI660C, Shanghai). The infrared irradiation (λ > 800 nm) was obtained by using an 800 nm highpass optical filter on the path of the simulated solar light. The electrochemical impedance spectroscopy (EIS) was performed on an electrochemical workstation (Zennium Zahner, Germany) under AM 1.5G, and the EIS Nyquist plots were measured at a bias of V_{oc} with ac amplitude of 10 mV under a frequency ranging from

Table 1
Detailed photovoltaic characteristics and dye-loading amount properties of DSSCs based on different photoelectrodes.

Samples	V_{oc} (V)	J_{sc} (mA cm^{-2})	FF (%)	η (%)	η (%) (λ > 800 nm)	Dye adsorption ($\times 10^{-3}$ mol m^{-2})	R_{ct2} (Ω)
Pure TiO_2	0.707	15.89	60.28	6.77	0.046	2.15	10.93
SYE	0.658	13.06	62.23	5.35	–	2.03	26.82
SYE@T	0.694	19.01	61.02	8.05	–	2.26	14.75
SY/A@T	0.690	19.94	62.32	8.58	–	2.27	–
SYE/A@T	0.694	20.94	59.48	8.64	0.232	2.27	15.38

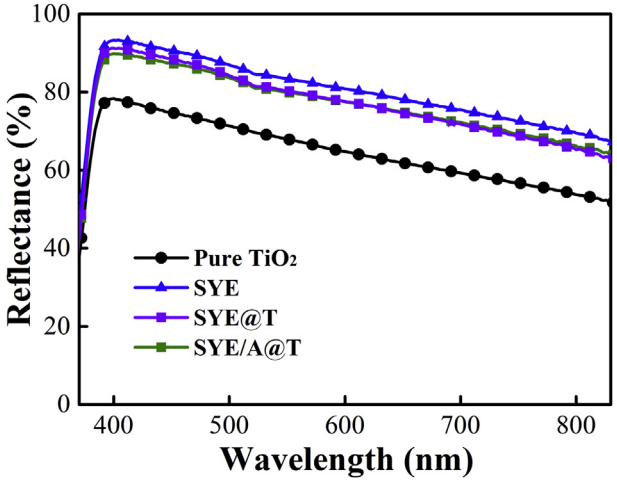

Fig. 5. UV–vis diffuse reflectance spectra in the visible region of different photoelectrodes.

10^{-1}–10^{5} Hz.

3. Results and discussion

3.1. Morphological and structure characterization

Fig. 2a and b are SEM images of as-prepared SYE, showing that the SYE exhibits a 3D starlike structure, and each single petal is apparently stacked with arrays of 1D smooth-faced nanorods. In order to reveal the morphology variation arising from Er doping, and Au NP attachment together with TiO_2 coating, SEM images of SY (Fig. 2c) and SYE/A@T (Fig. 2d) are also provided. One can see that these SY-based samples maintain analogous structure and morphology after introduction of foreign species. However, it is worth noting that upon being attached with Au nanoparticles (Au NPs) and coated with TiO_2, the surface of SYE/A@T become rougher, as shown in Fig. 2d. Such surface roughness variation originating from Au NPs attachment and TiO_2 coating can also be clearly observed by TEM images of SYE (Fig. 2e) and SYE/A@T (Fig. 2f). The high resolution TEM (HRTEM) images (Fig. 2g and h) provide more details of the SYE/A@T. From the low magnification HRTEM image (Fig. 2g), both attached Au NPs of ~8 nm and ~30 nm thick TiO_2 shell can be observed on the surface of the SYE. The high magnification HRTEM image (Fig. 2h) of the coating layer of SYE/A@T shows two typical interplanar distances of 0.235 nm and 0.350 nm, which are assigned to the (111) crystal plane of Au and (101) crystal plane of anatase TiO_2, respectively. Additionally, nano-sized internal pores within the shell of TiO_2 grains can be also observed, which is thought to be able to increase the dye-loading amount of photoelectrode. From EDS spectrum (Fig. 2i), peaks of host (Y and O) and dopant (Er) are detected for SYE/A@T composite, revealing the presence of Er atoms with a molar ratio of about 1: 10 to Y atoms, which accords with the molar ratio of reactant (1:10). In addition,

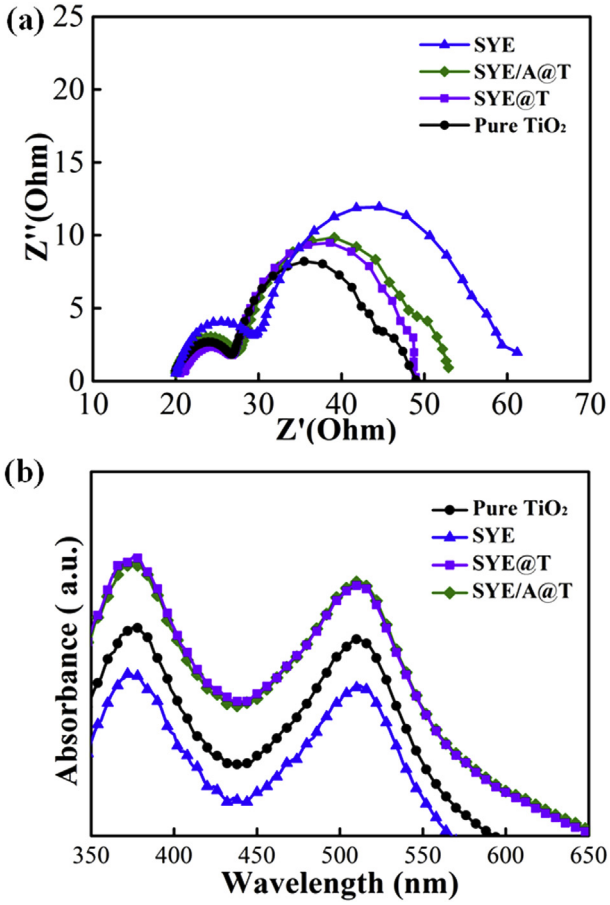

Fig. 6. (a) EIS Nyquist plots for DSSCs with different photoanodes obtained under AM 1.5G light and bias of V_{oc}. (b) UV–vis absorption spectra of the N719 dye in 0.1 M NaOH aqueous solution desorbed from different photoanodes.

relatively weak signals of Ti and Au are also discerned for SYE/A@T composite, further verifying the successful attachment of Au NPs and coating of TiO_2 on the SYE surface. Fig. 2j shows the XRD patterns of the SYE and SYE/A@T. The XRD diffraction peaks of both the SYE and SYE/A@T can be readily indexed to the pure cubic-phase Y_2O_3 (JCPDS 41-1105), indicating that either doping Er^{3+} or modifying with Au and TiO_2 does not change the crystal structure of Y_2O_3 since the ionic radii and coordination numbers of both Er and Y cations are very similar. The signals of Au and TiO_2 were too weak to detect in the XRD pattern of SYE/A@T owing to their low content and relative low crystallinity within the composite.

3.2. Photoluminescence property

The photoluminescence spectra of the as-synthesized SYE, SYE/A together with SYE/A@T excited with a λ = 980 nm laser, as displayed in Fig. 3a, reveal the influence of Au NPs and TiO_2 shell on

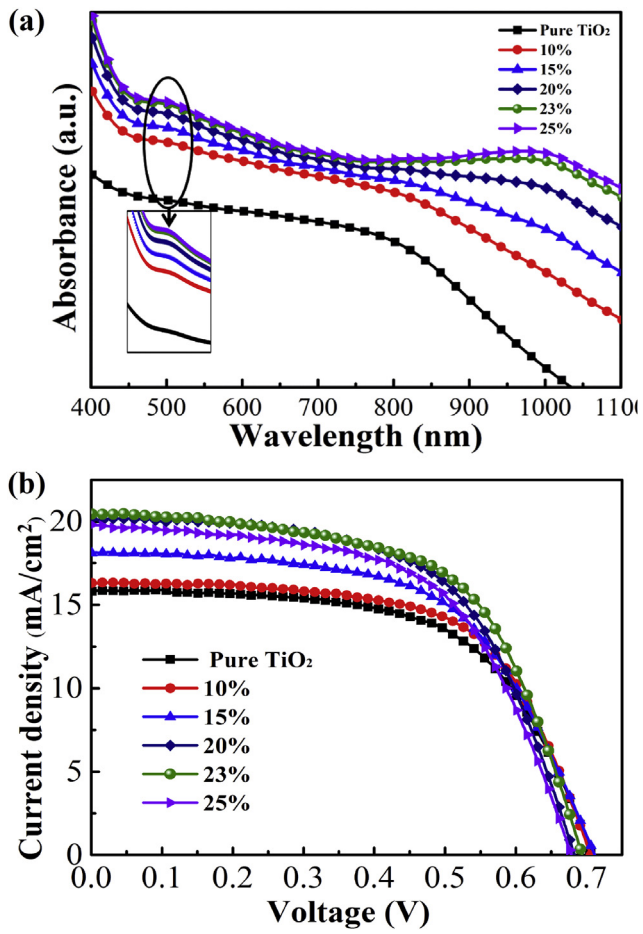

Fig. 7. (a) UV-vis absorption spectra of photoelectrodes with different weight ratio of SYE/A@T. (b) *J–V* curves of DSSCs with different weight ratios of SYE/A@T under AM 1.5G light.

the light emission of the SYE/A@T. The emission bands of SYE centered at 525, 560 nm, and 660 nm are attributed to the transition of the $^2H_{11/2}$, the $^4S_{3/2}$ and the $^4F_{9/2}$ excited states to the $^4I_{15/2}$ ground state of Er^{3+}, respectively, and this result is in agreement with the previous observation [41]. As shown in Fig. 3b, these luminescence bands well coincide with the absorption wavelength of N719 dye, indicating that the NIR light can be indirectly absorbed by N719 dye *via* UC process. In other words, incorporation of this SYE/A@T UC composite in DSSCs can be a feasible way to enhance the sunlight harvesting in NIR region. The enhancement of light absorption owing to extending photo-response region from visible to NIR is thought to be beneficial to the improvement of the photoelectric conversion performance of DSSC device. A possible schematic presentation for the conversion luminescence of Er^{3+} and the energy transfer from Er^{3+} to N719 dye has been provided in Fig. S1. As shown in Fig. 3a, when Au NPs were introduced by attaching on the SYE, the intensity of PL spectra of SYE/A increased appreciably. The enhancement of UC emission originating from Au NPs may be attributed to two possible interaction between SYE and Au NPs: (1) local electric field enhancement (LFE) and (2) surface-plasmon-coupled emission (SPCE) [42]. The LFE associated with plasmonic resonance can increase the excitation rate, that is, enhance the effective excitation flux [42]. For the SYE/A, the plasmon resonance band of the Au NPs (around 510 nm) does not match the excitation wavelength (980 nm). Therefore, the influence of LFE could be ignored in the SYE/A. As for SPCE, occurring upon the emission band of the fluorophore overlapping with the plasmonic resonance frequency of the metal nanostructures, it is reported to be able to increase the emission rate and thus enhance the emission efficiency due to the coupling of the UC emission with the plasmonic resonance [43]. UV–vis absorption spectrum of the Au NPs (Fig. 3b) clearly exhibits that the plasmonic resonance frequency of the Au NPs overlaps well with the green emission bands of SYE (525 nm and 560 nm), which allows the effective coupling of plasmonic resonance with UC emission and hence leads to an increment of the emission intensity. Such increased emission intensity *via* combination of SYE and Au NPs could ensure sufficient excitation for UC, and hence greatly enhance the final sunlight harvesting in N719 and improve the photoelectric conversion efficiency of DSSCs. Note that the Au NPs plasmonic resonance couples better with the green emission than the red, therefore the enhancement factor of the green emission is larger than that of the red one, as shown in Fig. 3c. Thus, UV–vis absorption spectra together with PL spectra verify that the SPCE plays a dominated role in the enhancement of UC emission. Furthermore, from the PL spectra it can be also found that TiO_2 shell causes a slightly decrease of the emission intensity of SYE/A. Such phenomenon might be attributed to two possible reasons. On one hand, TiO_2 has a higher phonon energy (about 600 cm^{-1}) than Y_2O_3 (about 550 cm^{-1}), leading to extra energy loss associated with the increasing probability of multiphonon nonradiative transition [44,45]. On the other hand, the rough TiO_2 shell can scatter part of incident NIR light and simultaneously absorb part of emissive visible light, hence resulting in the decrease of utilization of the NIR light.

3.3. Photovoltaic performance of DSSCs

In order to evaluate the optical properties and performances of DSSC doped with SYE/A@T, different double-layered photoelectrode films by printing a UC-TiO_2 (200 nm) scattering layer (SL) on the top of a TiO_2 (20 nm) transparent layer (TL) were constructed. As shown in Fig. S3, the thicknesses of TL and SL are measured to be 11 μm and 4 μm, respectively. For clarity, photoelectrode sample corresponding to the photoelectrodes added with SYE, SY/A@T, SYE@T, and SYE/A@T, respectively. For comparison, a pure TiO_2 photoelectrode (denoted as pure TiO_2) was also made in parallel. The photocurrent density-voltage (*J-V*) curves of all the DSSCs are shown in Fig. 4, and their photovoltaic parameters are summarized in Table 1. As can be seen, the pure TiO_2 cell exhibits a short-circuit current density (J_{sc}) of 15.89 mA cm^{-2} and a photoelectric conversion efficiency (η) of 6.77%, and the cell SYE shows the lowest J_{sc} of 13.06 mA cm^{-2} and η of 5.35%. As for SYE/A@T cell, the photovoltaic performance is improved and the highest J_{sc} of 20.94 mA cm^{-2} and η of 8.64% are achieved, which are 27.6% and 61.5% enhancements of η as compared with pure TiO_2 and SYE cells, respectively.

3.4. Scattering properties of photoelectrodes

To find out the reasons of the photovoltaic enhancement associated with the morphology as well as the components of the Au/TiO_2-modified UC composites, we measured UV–vis diffuse reflectance spectra of above photoelectrodes in the wavelength region of 400–800 nm, and the results are shown in Fig. 5. Comparing with pure TiO_2 film, all the UC-composite-doped photoelectrode films exhibit a remarkable improvement in light reflection over the entire region. Similarly, the reflectance of the photoelectrode increases with the increase of adding amount of SYE/A@T, as shown in Fig. S2a. These results reveal that the micron-sized UC composites can act as stronger light scattering centers than submicron-sized TiO_2 (200 nm) can. However, SYE cell

Table 2
Detailed photovoltaic characteristics and dye loading properties of DSSCs with different weight ratio of SYE/A@T under AM 1.5G light.

Samples	V_{oc} (V)	J_{sc} (mA cm^{-2})	FF(%)	η (%)	Dye adsorption ($\times 10^{-3}$ mol m^{-2})
Pure TiO_2	0.707	15.89	60.28	6.77	2.15
10%	0.706	16.34	62.26	7.18	2.17
15%	0.711	18.17	58.44	7.55	2.20
20%	0.683	20.18	59.20	8.16	2.25
23%	0.694	20.94	59.48	8.64	2.27
25%	0.678	19.81	58.04	7.80	2.30

performs much worse than SYE@T cell, SYE/A@T cell, and even pure TiO_2 cell. The low performance of SYE indicates that the introduction of bare UC materials makes negative effect on the DSSC performance. Such a negative effect might be associated with poor electron transport ability and poor dye-loading ability of bare SYE. In contrast, the SYE@T cell exhibits much better performance than the SYE cell. Therefore, the coated TiO_2 shell play an important role on the photoelectric behaviours of DSSC.

3.5. Electron transport and dye-loading abilities of photoelectrodes

To investigate the influence of TiO_2 shell out of SYE core on the photoelectric behaviours of DSSC, electrochemical impedance spectroscopy (EIS) was employed to examine the SYE, pure TiO_2 and SYE@T cells [46]. As shown in Fig. 6a, all the three plots exhibit two distinguishable semicircles, which are associated with the electrochemical reaction at the electrolyte/counter electrode interface in the10^3 Hz range (R_{ct1}) and at the TiO_2/dye/electrolyte interface in the $10^{-1}$to 10^3 Hz range (R_{ct2}) from left to right, respectively [47]. The electron transport property in the photoanode can be judged by R_{ct2}, which is defined by the diameter of the low-frequency semicircle [48,49]. According to the fitted values of R_{ct2} listed in Table 1, it can be seen that the impedance drastically increases from 10.93 Ω for the pure TiO_2 cell to 26.82 Ω for the SYE cell, implying a weak charge transport within the SYE cell. It may be attributed to the serious charge recombination effect and poor charge transport ability of bare SYE in the photoanodes, and hence a low electron diffusion and collection efficiency in the SYE cell [50]. Compared with the SYE cell, the impedance for the SYE@T cell dramatically decreased to 14.75 Ω, implying that the negative charge recombination originating from micron-sized SYE was remarkably reduced and the electron transport was improved by coating a TiO_2 shell. However, the charge transport in the SYE@T and SYE/A@T cell is still more difficult than in the pure TiO_2 cell, that is, introducing SYE@T or SYE/A@T still increases the impedance of photoanode film. Moreover, UV–vis absorption spectra of dye solution desorbed from the above N719-sensitized photoanodes were also measured to investigate the influence of TiO_2 shell on dye-loading ability, as shown in Fig. 6b, and the corresponding dye-loading amounts results are listed in Table 1. It can be seen that the introduction of bare SYE severely reduce the dye-loading amount of photoanode. After being coated with TiO_2 shell, the SYE@T as well as SYE/A@T could adsorb more dye molecules than SYE, attributed to the nanoporous structure of TiO_2 shell. That is, with the increase of SYE/A@T weight ratio, more and more dye molecules are adsorbed into the photoanode film, which can be identified by the dye-loading amount results in Fig. S2b. The increase in dye-loading amount can enhance the amount of photo-generated electrons and thereby contribute to a better photovoltaic performance of DSSCs.

3.6. Light-harvesting ability of photoelectrodes

Comparing the SYE@T cell with SYE/A@T cell, we can find a discernable difference in photovoltaic performance, indicating that Au NPs also play a notable role in improving the photovoltaic property of SYE/A@T. To understand the function of Au NPs, the light-harvesting ability of unsensitized SYE/A@T photoelectrodes with different adding amount of SYE/A@T were investigated by measuring the absorption spectra within the visible and NIR range of 400–1000 nm, as displayed in Fig. 7a. The percentages varying from 10% to 25% correspond to different mass-fractions of SYE/A@T with respect to scattering layer. Obviously, the absorption of the SYE/A@T is increasing with the increase of adding amount of SYE/A@T within the visible and NIR range of 400–1000 nm. Note that for all the SYE/A@T, the absorption increase within NIR region, especially in the wavelength around 980 nm indicates more NIR light could be exploited and transferred into absorbable photons for dye *via* UC process. As demonstrated in Fig. 4b, the η of SYE/A@T cell under NIR irradiation (λ > 800 nm) is much higher than that of pure TiO_2. However, this increase owing to UC effect under NIR irradiation cannot account for the total increase of η from the pure TiO_2 to SYE/A@T (compare Fig. 4a and b). Thus, it means that the extension of light-harvesting band to NIR region caused by plasmon-enhanced UC effect makes an almost negligible contribution to the total increase of η of SYE/A@T. Moreover, an absorption enhancement in the wavelength around 515 nm owing to the LSPR effect of Au NPs is discerned for all the SYE/A@T [42]. It is worth noting that such absorption of Au NPs within SYE/A@T (Fig. 7a) shows a slight red shift versus the absorption the pure Au NPs displayed in Fig. 3b, which is arising from the aggregation of Au NPs [42,43]. Under sunlight irradiation, the plasmon-induced electrons in the Au NPs of SYE/A@T could move through Au-TiO_2 interface into the conduction band of TiO_2 [51]. Therefore, the absorption enhancement in the wavelength of about 515 nm is thought to be beneficial for the enhancement of DSSC performance by attaching Au NPs.

Based on the above results, on one hand, the addition of SYE/A@T in the TiO_2 photoelectrode is able to improve the light harvest of DSSC by increasing dye-loading amount, light reflectance and LSPR effect of Au NPs, facilitating achieving a better cell performance. On the other hand, the introduction of SYE/A@T in the TiO_2 photoelectrode is unfavourable for the charge transport within the photoanode film. In order to precisely determine the optimized adding amount of SYE/A@T for attaining a high η, SYE/A@T cells with different weight ratios of SYE were also assembled and characterized, as shown in Fig. 7b and Table 2. It is found that the 23% SYE/A@T cell yields a maximum J_{sc} (20.94 mA cm^{-2}) and η (8.64%) among a series of SYE/A@T adding amount of 0%, 10%, 15%, 20%, 23% and 25%.

4. Conclusions

In summary, 3D starlike core-shell-structured Y_2O_3:Er/Au@TiO_2 composite was prepared and demonstrated effective upconversion and light scattering when applied in DSSC. The TiO_2 shell out of the upconversion core remarkably reduced the charge recombination on the surface of SYE and simultaneously enlarged the dye-loading amount. In addition, the LSPR effect originating from Au NPs can

not only intensify the upconversion emission intensity *via* SPCE, but also enhance the light absorption around wavenumber of 515 nm. At the optimum mixing weight ratio of 23%, an efficiency of 8.64% was obtained, which was a significant improvement of 27.6% compared with the pure TiO_2 cell. Our work provides a feasible strategy to prepare an upconversion composite with plasmon-enhanced emission and enable this composite to accommodate the DSSCs system and improve the conversion efficiency of DSSCs.

Acknowledgements

The work was supported by the National Natural Science Foundation of China (Nos. 21176019, 21377011, 21476019), 863 project (2013AA031901), and Beijing Higher Education Young Elite Teacher Project (YETP0487).

Appendix A. Supplementary data

Supplementary data related to this article can be found at http://dx.doi.org/10.1016/j.jpowsour.2016.03.032.

References

[1] B. O'Regan, M. Graetzel, Nature 353 (1991) 737–740.
[2] M. Grätzel, Acc. Chem. Res. 42 (2009) 1788–1798.
[3] M.K. Nazeeruddin, F. De Angelis, S. Fantacci, A. Selloni, G. Viscardi, P. Liska, S. Ito, B. Takeru, M. Grätzel, J. Am. Chem. Soc. 127 (2005) 16835–16847.
[4] F. Gao, Y. Wang, D. Shi, J. Zhang, M. Wang, X. Jing, R. Humphry-Baker, P. Wang, S.M. Zakeeruddin, M. Gratzel, J. Am. Chem. Soc. 130 (2008) 10720–10728.
[5] A. Yella, H.-W. Lee, H.N. Tsao, C. Yi, A.K. Chandiran, M.K. Nazeeruddin, E.W.-G. Diau, C.-Y. Yeh, S.M. Zakeeruddin, M. Grätzel, Science 334 (2011) 629–634.
[6] S. Mathew, A. Yella, P. Gao, R. Humphry-Baker, B.F. Curchod, N. Ashari-Astani, I. Tavernelli, U. Rothlisberger, M.K. Nazeeruddin, M. Grätzel, Nat. Chem. 6 (2014) 242–247.
[7] A. Hagfeldt, G. Boschloo, L. Sun, L. Kloo, H. Pettersson, Chem. Rev. 110 (2010) 6595–6663.
[8] S.K. Balasingam, M. Lee, M.G. Kang, Y. Jun, Chem. Commun. 49 (2013) 1471–1487.
[9] J.-H. Yum, E. Baranoff, S. Wenger, M.K. Nazeeruddin, M. Grätzel, Energy Environ. Sci. 4 (2011) 842–857.
[10] M.K. Nazeeruddin, P. Pechy, T. Renouard, S.M. Zakeeruddin, R. Humphry-Baker, P. Comte, P. Liska, L. Cevey, E. Costa, V. Shklover, J. Am. Chem. Soc. 123 (2001) 1613–1624.
[11] C.-M. Lan, H.-P. Wu, T.-Y. Pan, C.-W. Chang, W.-S. Chao, C.-T. Chen, C.-L. Wang, C.-Y. Lin, E.W.-G. Diau, Energy Environ. Sci. 5 (2012) 6460–6464.
[12] S.-Q. Fan, C. Kim, B. Fang, K.-X. Liao, G.-J. Yang, C.-J. Li, J.-J. Kim, J. Ko, J. Phys. Chem. C 115 (2011) 7747–7754.
[13] H. Choi, S. Kim, S.O. Kang, J. Ko, M.S. Kang, J.N. Clifford, A. Forneli, E. Palomares, M.K. Nazeeruddin, M. Grätzel, Angew. Chem. Int. Ed. 47 (2008) 8259–8263.
[14] J.-H. Yum, S.-R. Jang, P. Walter, T. Geiger, F. Nüesch, S. Kim, J. Ko, M. Grätzel, M.K. Nazeeruddin, Chem. Commun. (2007) 4680–4682.
[15] G. Sharma, S.P. Singh, R. Kurchania, R. Ball, RSC Adv. 3 (2013) 6036–6043.
[16] J. Zhou, Q. Liu, W. Feng, Y. Sun, F. Li, Chem. Rev. 115 (2014) 395–465.
[17] G. Chen, H. Qiu, P.N. Prasad, X. Chen, Chem. Rev. 114 (2014) 5161–5214.
[18] H.Q. Wang, M. Batentschuk, A. Osvet, L. Pinna, C.J. Brabec, Adv. Mater. 23 (2011) 2675–2680.
[19] J.-L. Wu, F.-C. Chen, S.-H. Chang, K.-S. Tan, H.-Y. Tuan, Org. Electron. 13 (2012) 2104–2108.
[20] Z. Zhou, J. Wang, F. Nan, C. Bu, Z. Yu, W. Liu, S. Guo, H. Hu, X.-Z. Zhao, Nanoscale 6 (2014) 2052–2055.
[21] G.B. Shan, G.P. Demopoulos, Adv. Mater. 22 (2010) 4373–4377.
[22] J. Wu, J. Wang, J. Lin, Z. Lan, Q. Tang, M. Huang, Y. Huang, L. Fan, Q. Li, Z. Tang, Adv. Energy Mater. 2 (2012) 78–81.
[23] J. Wang, J. Lin, J. Wu, M. Huang, Z. Lan, Y. Chen, S. Tang, L. Fan, Y. Huang, Electrochim. Acta 70 (2012) 131–135.
[24] Y. Li, K. Pan, G. Wang, B. Jiang, C. Tian, W. Zhou, Y. Qu, S. Liu, L. Feng, H. Fu, Dalton Trans. 42 (2013) 7971–7979.
[25] X.-H. Lu, Y.-Z. Zheng, S.-Q. Bi, J.-X. Zhao, X. Tao, J.-F. Chen, J. Power Sources 243 (2013) 588–593.
[26] J.-C. Boyer, F.C. Van Veggel, Nanoscale 2 (2010) 1417–1419.
[27] L. Sudheendra, V. Ortalan, S. Dey, N.D. Browning, I.M. Kennedy, Chem. Mater. 23 (2011) 2987–2993.
[28] M. Saboktakin, X. Ye, S.J. Oh, S.-H. Hong, A.T. Fafarman, U.K. Chettiar, N. Engheta, C.B. Murray, C.R. Kagan, ACS Nano 6 (2012) 8758–8766.
[29] M. Saboktakin, X. Ye, U.K. Chettiar, N. Engheta, C.B. Murray, C.R. Kagan, ACS Nano 7 (2013) 7186–7192.
[30] L. Li, K. Green, H. Hallen, S.F. Lim, Nanotechnology 26 (2015) 025101.
[31] N. Liu, W. Qin, G. Qin, T. Jiang, D. Zhao, Chem. Commun. 47 (2011) 7671–7673.
[32] P. Yuan, Y.H. Lee, M.K. Gnanasammandhan, Z. Guan, Y. Zhang, Q.-H. Xu, Nanoscale 4 (2012) 5132–5137.
[33] P. Zhao, Y. Zhu, X. Yang, X. Jiang, J. Shen, C. Li, J. Mater. Chem. A 2 (2014) 16523–16530.
[34] H.-X. Mai, Y.-W. Zhang, L.-D. Sun, C.-H. Yan, J. Phys. Chem. C 111 (2007) 13721–13729.
[35] F. Wang, J. Wang, X. Liu, Angew. Chem. 122 (2010) 7618–7622.
[36] M. Haase, H. Schäfer, Angew. Chem. Int. Ed. 50 (2011) 5808–5829.
[37] J. Chang, Y. Ning, S. Wu, W. Niu, S. Zhang, Adv. Funct. Mater. 23 (2013) 5910–5915.
[38] G.-B. Shan, H. Assaaoudi, G.P. Demopoulos, ACS Appl. Mater. Interfaces 3 (2011) 3239–3243.
[39] P. Ramasamy, J. Kim, Chem. Commun. 50 (2014) 879–881.
[40] L. Liang, Y. Liu, C. Bu, K. Guo, W. Sun, N. Huang, T. Peng, B. Sebo, M. Pan, W. Liu, Adv. Mater. 25 (2013) 2174–2180.
[41] F. Vetrone, J.C. Boyer, J.A. Capobianco, A. Speghini, M. Bettinelli, Chem. Mater. 15 (2003) 2737–2743.
[42] H. Zhang, Y. Li, I.A. Ivanov, Y. Qu, Y. Huang, X. Duan, Angew. Chem. 122 (2010) 2927–2930.
[43] J.R. Lakowicz, Plasmonics 1 (2006) 5–33.
[44] Z. Pan, S.H. Morgan, K. Dyer, A. Ueda, H. Liu, J. Appl. Phys. 79 (1996) 8906–8913.
[45] J. Capobianco, J. Boyer, F. Vetrone, A. Speghini, M. Bettinelli, Chem. Mater. 14 (2002) 2915–2921.
[46] Y.-H. Lai, C.-Y. Lin, H.-W. Chen, J.-G. Chen, C.-W. Kung, R. Vittal, K.-C. Ho, J. Mater. Chem. 20 (2010) 9379–9385.
[47] S.J. Lim, Y.S. Kang, D.-W. Kim, Electrochem. Commun. 12 (2010) 1037–1040.
[48] S. Yodyingyong, Q. Zhang, K. Park, C.S. Dandeneau, X. Zhou, D. Triampo, G. Cao, Appl. Phys. Lett. 96 (2010) 073115.
[49] J. Zhang, W. Que, Q. Jia, P. Zhong, Y. Liao, X. Ye, Y. Ding, J. Alloys Compd. 509 (2011) 7421–7426.
[50] Y.-Z. Zheng, X. Tao, L.-X. Wang, H. Xu, Q. Hou, W.-L. Zhou, J.-F. Chen, Chem. Mater. 22 (2009) 928–934.
[51] L. Du, A. Furube, K. Yamamoto, K. Hara, R. Katoh, M. Tachiya, J. Phys. Chem. C 113 (2009) 6454–6462.